HTML ABSTRACT + LINKS

JOURNAL OF APPLIED PHYSICS VOLUME 96, NUMBER 1 1 JULY 2004

Atomic level scanning transmission electron microscopy characterization of GaN/AlN quantum wells

K. A. Mkhoyan,[a] E. J. Kirkland, and J. Silcox
School of Applied and Engineering Physics, Cornell University, Ithaca, New York 14853

E. S. Alldredge
Physics Department, Cornell University, Ithaca, New York 14853

(Received 30 January 2004; accepted 6 April 2004)

GaN quantum wells in an AlN matrix are characterized using scanning transmission electron microscopy. The width of the quantum wells and sharpness of the interfaces are measured with composition sensitive annular dark field imaging and electron energy-loss spectroscopy. The effects of beam broadening inside the specimen are discussed and mechanisms to minimize it are suggested. The quantitatively measured intensity of the N K-edge versus position is compared with the propagating beam intensity obtained from multislice calculations. Possible effects of strain in the structure on its electronic states and energy-loss spectra are also discussed. © *2004 American Institute of Physics.* [DOI: 10.1063/1.1756222]

I. INTRODUCTION

The characterization of nanometer size structures (quantum wires, quantum dots, heterostructures, nanotubes, etc.) requires special analytic instrumentation with high spatial resolution. Scanning transmission electron microscopy (STEM) with a focused probe ~2 Å, equipped with an electron energy loss spectrometer (EELS) is often the instrument of choice.[1–5] However, despite the fact that in STEM an electron beam can be focused to ~2 Å or even to 0.8 Å in an aberration corrected STEM,[6] beam spreading inside the specimen due to interaction of the incident electrons with atoms of the specimen is unavoidable. Beam spreading typically introduces extra broadening of the measured profiles, for example, when chemical composition is measured, and does not affect the qualitative picture of the analysis. But, in cases where quantitative analysis is needed the effects due to beam spreading should be analyzed as well. The analysis of beam spreading will also suggest mechanisms to minimize it for direct measurements of the nanostructures.

In an earlier article,[7] we reported atomic level EELS measurements of the composition and uniformity of GaN/AlN multiple quantum wells (QWs). The results were accompanied with annular dark field (ADF) images of the structure. However, several questions remained unanswered. First, are the Gaussian-like profiles of the EELS data and ADF intensities indications that the interfaces were not atomically sharp or can they be attributed to a beam spreading effect? Second, how large was the effect of beam spreading on the composition analysis of the QWs.

In the QWs where the lattice constants of the materials constituting the well and the buffer are different, strain in the structure is expected. It is also known that the characteristic fine structure of the core-level energy-loss spectra of the material under strain can significantly differ from the relaxed equivalents.[8] These observations stress the importance of understanding the possible effects of strain on the EELS analysis of these GaN/AlN QWs.

In this article, the effects of beam broadening on STEM measurements of the GaN/AlN multiple quantum wells reported earlier by Mkhoyan *et al.*[7] are presented. A discussion of the mechanisms and parameters to minimize these effects will follow. Possible strain effects on the measured EELS data are also presented.

II. EXPERIMENT

The GaN/AlN QWs studied here were grown in a molecular beam epitaxy system on 2 in. c-plane sapphire wafers on which 0.3–0.5 μm AlN buffer layers were initially deposited.[9] The structure consists of 20 GaN/AlN QWs with 60 Å AlN barrier layers and about 12 Å GaN wells. Cross-sectional specimens for the STEM were prepared from these wafers by a tripod polishing technique.[10] Brief, low concentration (~10%) HF dipping was applied to the specimen to remove any remaining colloidal silica before loading into STEM. The Cornell 100 keV VG HB501 STEM used in these measurements has a field emission gun and a high resolution pole piece with a spherical aberration coefficient $C_s = 1.3$ mm chromatic aberration coefficient $C_c \sim 1.5$ mm, and a focused incident beam of ~2 Å with convergent angle of ~10 mrad (objective angle). Microscope is also equipped with electron spectrometer for EELS and was operated for electrons scattered into ~20 mrad collection aperture (collection angle). The measured energy resolution is 0.5 to 0.7 eV with an energy drift of <0.03 eV/min and an objective lens stability of ~1 ppm.[11]

A single QW was mapped[7] with approximately 3.3 Å steps by probing changes in the energy-loss spectra of the Ga $L_{2,3}$-edge and the N K-edge. First, changes in the integrated intensity of the Ga $L_{2,3}$-edge were measured across the well. Then, changes in the fine structure of the N K-edge and the ADF intensity were measured. The results are summarized in Figs. 1(a)–1(d). The ADF image illustrates the

[a]Electronic address: kam55@cornell.edu

 © 2004 American Institute of Physics

Downloaded 16 Sep 2008 to 134.84.147.97. Redistribution subject to AIP license or copyright; see http://jap.aip.org/jap/copyright.jsp

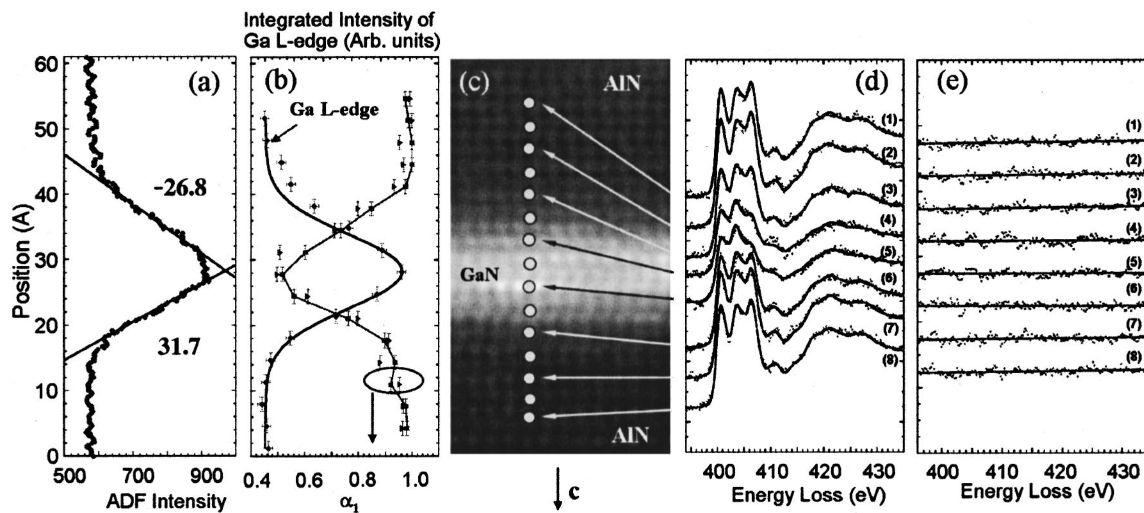

FIG. 1. Analysis of a GaN QW in an AlN matrix with ~2 Å focused electron beam [the dots in (c) represent the probe positions for the spectra in (d)]: (a) intensity of ADF signal and linear fit with the slopes; (b) integrated intensity of Ga $L_{2,3}$-edge and coefficient α_1 related to the relative concentration of AlN found from the N *K*-edge (see text); (c) high resolution ADF image of the GaN QW (with Wiener filter); (d) spectra of N *K*-edge recorded across the QW with their best fits, and (e) difference between recorded and best fit spectra on these *K*-edges.

Z-contrast effect. Ga has a much higher atomic number than Al or N. It produces a much higher signal (i.e., scattering at high angle) resulting in a bright horizontal band in Fig. 1(c) for the GaN quantum well. Relatively large 3.3 Å steps were chosen to avoid beam induced damage of the specimen. A thickness d of 470±50 Å was measured for this sample, using low-loss EELS, with $d \approx \lambda_{PL} \times I_{PL}/I_{ZL}$. Here I_{PL} and I_{ZL} are the plasmon-loss and zero-loss intensities, and λ_{PL} is the mean-free path for plasmon generation. The calculated mean-free path for plasmon generation in AlN is $\lambda_{PL}^{AlN} \simeq 94$ nm.[12]

The recorded spectra of the N *K*-edge, measured across the well, were fitted to a linear combination of two normalized spectra of the N *K*-edge in bulk AlN and GaN

$$I_s = \alpha_1 I_{AlN} + \alpha_2 I_{GaN}, \quad (1)$$

using a linear least-squares curve fitting algorithm.[13] The weighting coefficients α_1 and α_2 are a measure of the relative material type. Some of these recorded spectra with their best fits are presented in Fig. 1(d). The normalized coefficient α_1 [$\alpha_1 \leftarrow \alpha_1/(\alpha_1+\alpha_2)$] from two sets of data are presented in Fig. 1(b).

The application of a linear combination of two spectra of the bulk material to the spectra measured across the QW is valid under the assumption that the *K*-edge spectra from the N atoms are primarily determined by the first neighbor atoms (Ga and/or Al atoms). The validity of this assumption is evident from the results. As can be seen from Fig. 1(e) the differences between the recorded spectra and the linear combination fits are primarily noise. This demonstrates that the spectra from the interfacial N atoms, which have Ga and Al neighbor atoms, do not contain any major new features.

To perform a least-squares curve fit, reference N *K*-edge spectra measured in AlN and GaN were obtained under identical conditions and crystal orientation as the ones measured across the well. Then these two spectra were normalized to have the same intensity 35 eV above the edge onset. These reference spectra are presented in Fig. 2. It should be stressed here that the wurtzite forms of AlN and GaN are uniaxial crystals and the fine structure of the N *K*-edge in the direction of the *c*-axis and perpendicular to it differ significantly.[14] Therefore, the requirement of having these reference spectra measured under the exact same conditions and crystal orientation is essential. For details on the orientation dependent fine structure of the N *K* edge in the AlN and GaN see Refs. 14 and 15.

The results of the measurements (see Fig. 1) indicate that the GaN QW is not symmetric around the center. The first interface (starting from the substrate) is about two monolayers broader than the second. This is most likely due to the presence of a surface roughness in AlN buffer layers grown at low temperatures.

From the STEM characterization point of view there are two interesting observations in Fig. 1. First, the coefficient α_1 (proportional to AlN concentration) in the center of the QW, which is GaN, is not 0 (or close to 0), but is ~0.5; second, the ADF intensity (proportional to the GaN concentration) and EELS profiles of the QWs follow a Gaussian

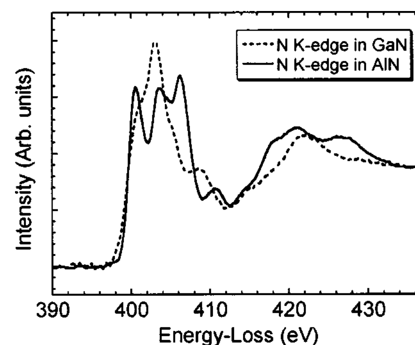

FIG. 2. Measured energy loss spectra of the N *K*-edge in wurtzite GaN and AlN. Each curve is normalized to have the same intensity 35 eV above the edge onset.

Downloaded 16 Sep 2008 to 134.84.147.97. Redistribution subject to AIP license or copyright; see http://jap.aip.org/jap/copyright.jsp

function rather than a rectangular function. These observations are the results of incident beam broadening inside the heterostructures and will be discussed in detail in the following section.

One of the critical parameters in exploration of beam spreading inside the sample is specimen thickness and, therefore, the sensitivity of beam broadening to specimen thickness will be discussed as well.

III. CALCULATIONS

The multislice method[16,17] for calculation of the propagation of the incident electron beam through the specimen has been successfully used to understand some experimental observations. A good match between calculated and measured relative contrast levels of crystal lattice fringes as a function of defocus,[18] and simulated convergence-beam electron diffraction patterns with measured ones[19,20] have been reported. Multislice methods were used here to describe the effects of beam broadening in the GaN/AlN QWs.

A. Multislice calculations

A supercell containing a single GaN/AlN QW was used for the multislice simulations. Four monolayers of GaN were introduced within bulk AlN to produce a ~12 Å GaN QW in an AlN matrix (four monolayers of GaN surrounded with six monolayers of AlNs on both sides). The supercell was aligned so that the incident beam is parallel to the $[\bar{2}110]$ crystallographic direction. As can be seen from Fig. 1(c) this is also the direction of the incident beam in the experi ments. The supercell size was 37.7 Å×39.8 Å, sampled with 1024×1024 pixels. A section of this supercell is presented in Fig. 3.

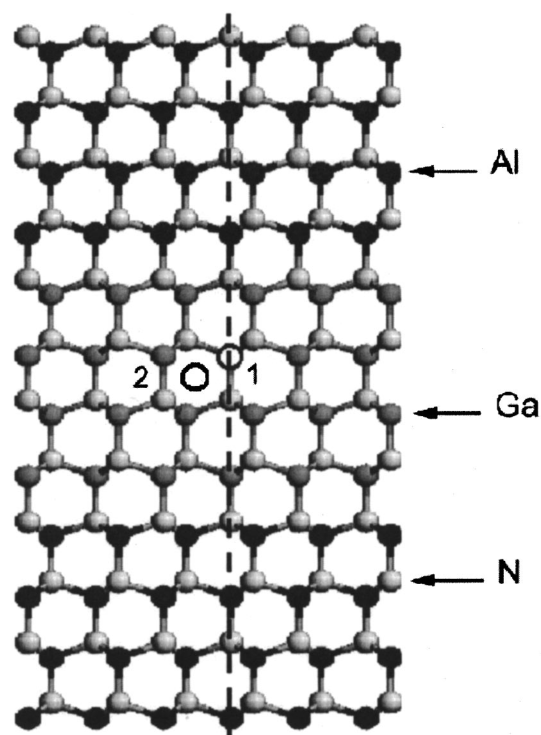

FIG. 3. A section of the supercell representing a GaN QW in an AlN matrix. The circles labeled 1 and 2 indicate the positions of the incident STEM probe in *on* and *off* axis simulations. The probe positions in Fig. 1 are indicated with a dashed line.

The incident beam and its propagation at different thicknesses in the specimen were calculated using a multislice simulation program.[21] This code is based on alternately passing an incident beam through a thin slice of the specimen and propagation between slices.[16] In all calculations in this article, a single slice has a thickness of 1.555 Å. The electron optical parameters describing the ~2 Å incident electron probe in the STEM were 100 kV acceleration voltage, spherical aberration of $C_s = 1.3$ mm, objective angle of 10.0 mrad, and defocus of 700 Å.

B. Results and Discussion

Because the incident beam coincides with a crystallographic orientation, strong beam channeling[22] was expected. Two extreme cases of beam positioning in the crystal were considered (see Fig. 3). In the first case a focused STEM probe was located on the atomic column at position (1) (because Ga atoms scatter more strongly than N, the beam was located on the column consisting only of Ga atoms). In the second case, the beam was located between the columns at position (2). The results of the simulations indicating strong channeling for both cases are presented in Figs. 4 and 5. As can be seen in Fig. 4 at the beginning, when the probe is located on the Ga column, it is strongly focused on the column and then, with further penetration of the beam inside the specimen, dechanneling of the initial intensity to the neighboring columns takes place, broadening the probe area. In the second case, when the probe is located in between the columns (see Fig. 5), the channeling effect is more pronounced. For details on electron beam channeling in crystalline materials see Refs. 22 and 23.

To calculate some effects of beam broadening on the EELS profile measurements, the intensity of the propagating beam should first be projected (or integrated) along the QW (i.e., integrated along a horizontal direction parallel to the bright band in the center of Fig. 1(c)). Because the QWs are uniform along their growth plane, the portions of the beam which spread along the QW contribute to the EELS spectra in the same way. The integrated intensities of the STEM probe at different thicknesses are presented in Fig. 6(a), for the case where the incident probe is located on the column (position 2 in Fig. 3). The total EELS signal is the integral over the whole area of the probe, which may be partly inside the QW and partly outside even though it started completely inside the QW. To estimate this delocalization caused by channeling, the intensity profile in Fig. 6(a) is integrated perpendicular to the QW [i.e., in a vertical direction in Fig. 1(c)]. The total integrated intensity versus position perpendicular to the QW (relative to the incident position) is shown in Fig. 6(b) for different thicknesses. This is an estimate of the fraction of the incident beam that produces an EELS signal from different parts of the QW. (Phonons were not included in either of these calculations.)

To determine the fraction of the EELS signal that reflects a single layer, it is necessary to calculate the fraction of the intensity from the original probe that stays within a single

Downloaded 16 Sep 2008 to 134.84.147.97. Redistribution subject to AIP license or copyright; see http://jap.aip.org/jap/copyright.jsp

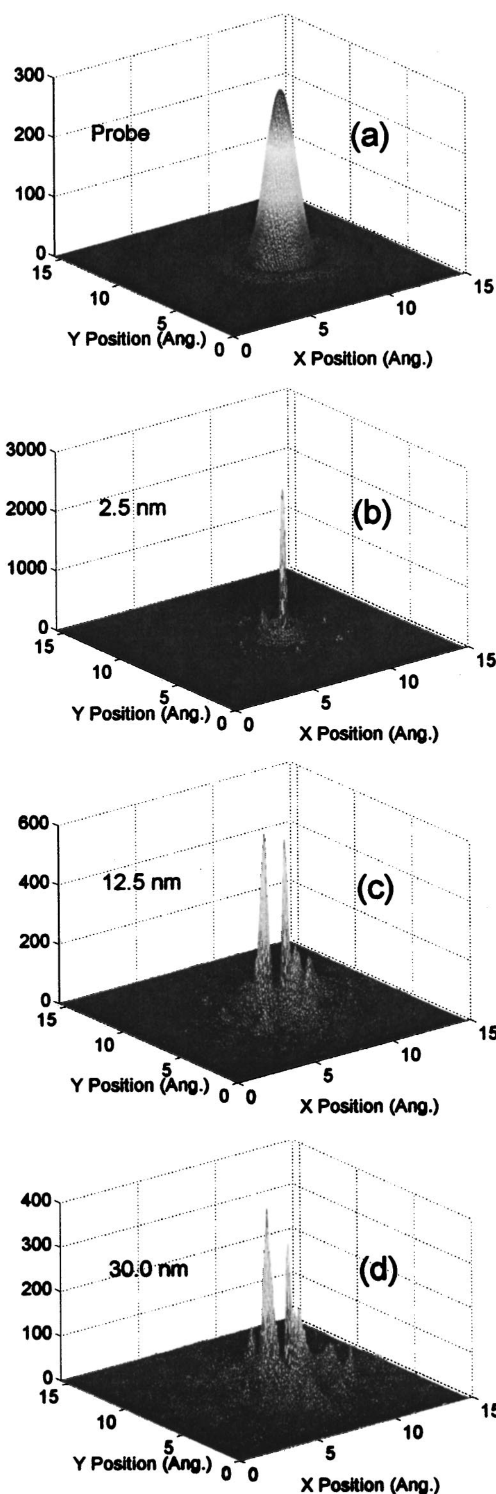

FIG. 4. Electron beam channeling along the $[\bar{2}110]$ crystallographic orientation in wurtzite GaN/AlN QW for 2.5, 12.5, and 30.0 nm penetration depths. An incident beam is located on the column of Ga atoms at position 1 in Fig. 3.

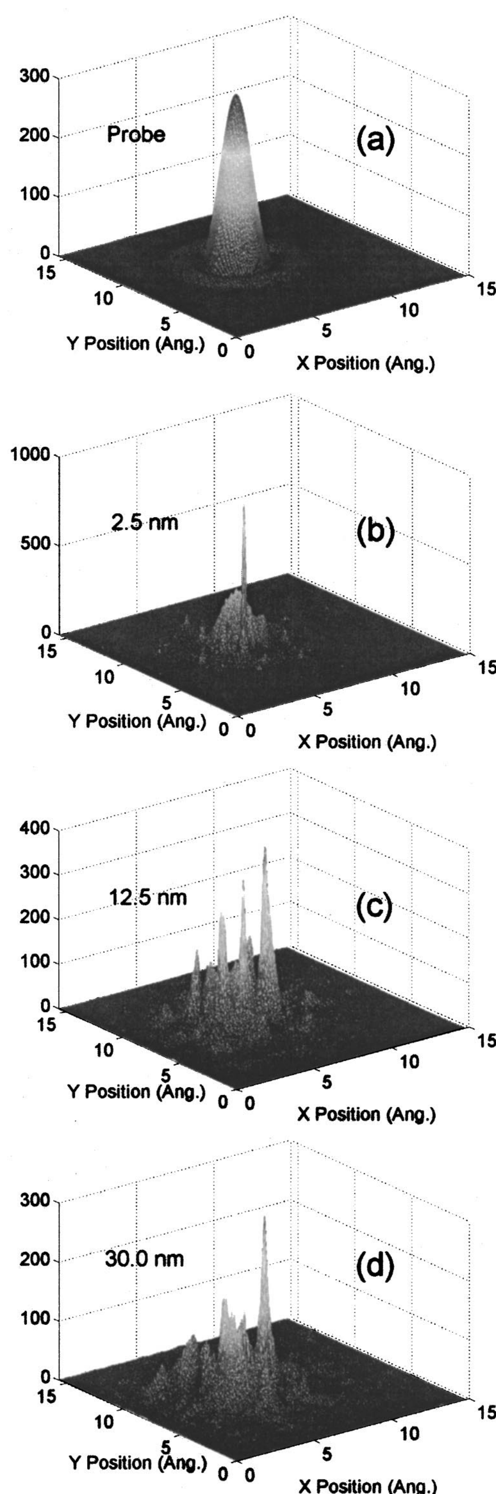

FIG. 5. Electron beam channeling along the $[\bar{2}110]$ crystallographic orientation in wurtzite GaN/AlN QW for 2.5, 12.5, and 30.0 nm penetration depths. An incident beam is located between the columns at position 2 in Fig. 3.

layer, i.e., within a 2.5 Å layer in this case. The variation of this intensity with penetration depth is presented in Fig. 7, where both cases of the probe position (on and off the atomic column, see Fig. 3) are considered. To calculate the fraction of the signal that represents the QW, the intensity of the beam should be integrated over the range covered by the GaN (see Fig. 3). The results of these calculations are also presented in Fig. 7.

It should be stressed that, as can be seen from Figs. 7(a) and 7(b), even at zero thickness the fraction of the beam that is in a single atomic layer (within 2.5 Å) is about 70% and after passing through 200 Å only about 40% of the intensity

Downloaded 16 Sep 2008 to 134.84.147.97. Redistribution subject to AIP license or copyright; see http://jap.aip.org/jap/copyright.jsp

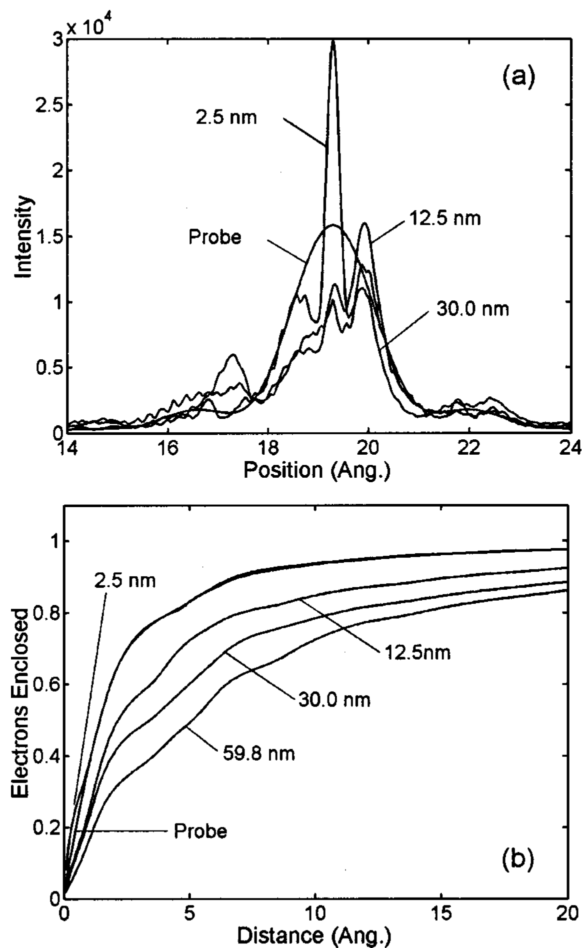

FIG. 6. (a) Calculated intensities of the propagated beam projected along the QW with the beam in position 2 (versus position perpendicular to the QW), and (b) the intensity of the propagated beam integrated perpendicular to the QW relative to the point of the incidence beam at different thicknesses.

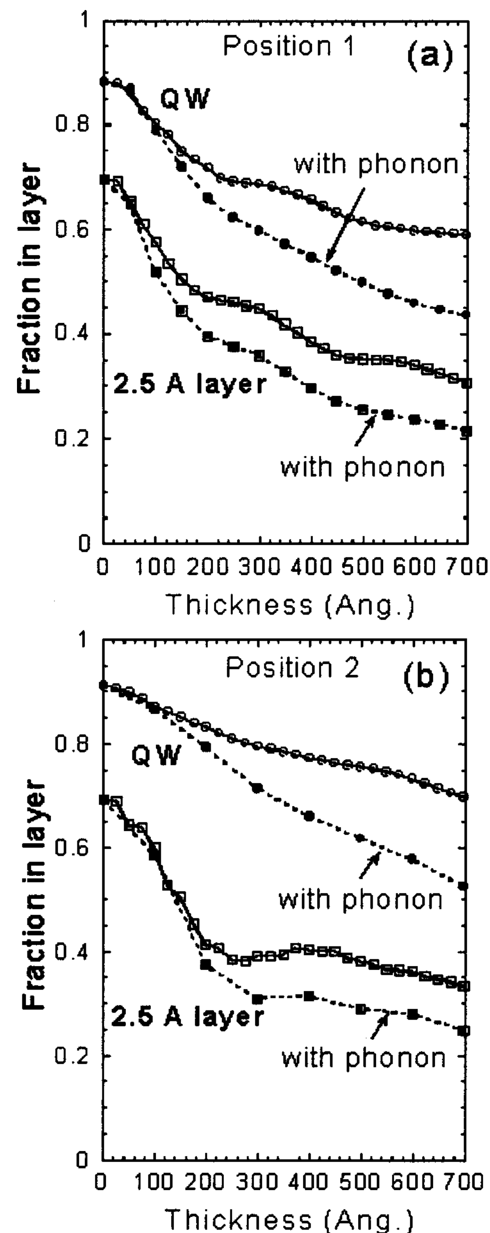

FIG. 7. Integrated intensity (calculated) of the electron beam in a single layer (2.5 Å) and in the GaN QW (beam position near center of QW) as a function of the penetration depth. Results of the calculations with and without phonons (room temperature) are shown.

remains in a single layer. The simple geometrical depth of focus for these optical conditions is approximately $\Delta z \sim \Delta x/\alpha \sim 250$ Å (where α is the objective semiangle), so much of this spreading is due to the specimen itself. These results indicate that STEM measurements (with similar instruments) cannot be easily interpreted as *direct* atomic level measurements and must be accompanied with appropriate numerical simulations of the beam transformation inside the specimen. Also note that, despite the fact that channeling of the incident beam and its spreading depends on the type of atoms, crystal structure, lattice constants, and direction of incidence and can be stronger or weaker, the broadening of the beam will always take place and should be considered with great care if atomic level analysis is needed. This situation may change with a smaller probe.

All the multislice calculations presented to this point were performed under the assumption that the atoms in the specimen were stationary. However, at room temperature, the atoms vibrate. The importance of including these vibrations (or phonons) in simulations for quantitative comparison to experimental observations has been shown previously.[19,20] The frozen phonon[19] method, which models phonons by randomly displacing atoms from their atomic site using a Gaussian distribution, was used here to model the thermal vibrations of the atoms of specimen. The results of these simulations are also presented in Fig. 7. As can be seen, the effects of the phonons become more significant with increasing beam penetration depth. These results [see Figs. 7(a) and 7(b)] indicate that up to a thickness of $\sim$100 Å the effects due to phonons are negligible. However, for a thickness $\geqslant$200 Å, the contributions from phonons are not small and cannot be ignored.

The next step in the simulations was to map the GaN QW by moving an incident probe across the QW with 1 Å steps and calculate the fraction of the beam in the QW at each step. Calculations were performed for a 470 Å thick sample including phonons. The fraction of the normalized integrated intensities in the GaN QW are shown in Fig. 8, where for comparison the profile of the coefficient α_1 from

Downloaded 16 Sep 2008 to 134.84.147.97. Redistribution subject to AIP license or copyright; see http://jap.aip.org/jap/copyright.jsp

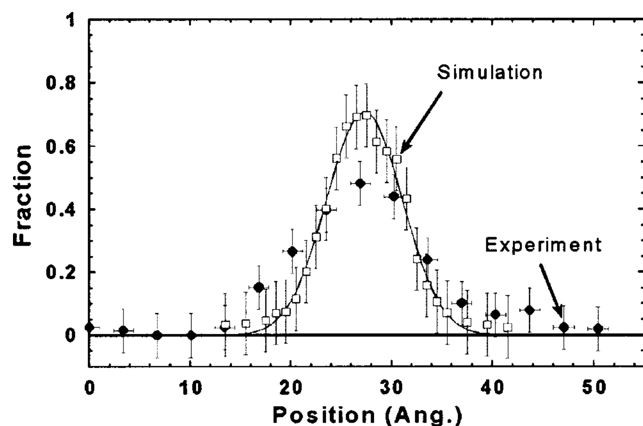

FIG. 8. Calculated fraction of the beam inside the QW vs incident beam position. The coefficient $(1-\alpha_1)$ from Fig. 1(b) is also presented. The results of the calculations were fit with a Gaussian function (solid line).

Fig. 1(b) is also presented. There error bars reflect the possibility that the incident beam may be slightly on or off of an atomic column.

Comparison between the calculated beam fraction inside the QW (Fig. 8) and α_1 yields the following observations. First, the Gaussian shape of the interface is simply due to beam broadening. Second, it suggests that one interface between the GaN well and the AlN is two monolayers wider than the other (this is still within the error bars so is not conclusive). Note that several factors might prevent an even stronger correlation between coefficient α_1 and the calculated beam fraction in the QW. From the experimental side, background subtraction (an E^r fit in the preedge was used to subtract the background of the N K-edge from the recorded EEL data) and least-squares fitting, which fits the entire spectrum, can introduce up to a 5%–7% error in value of α_1. From the simulation side, as in the discussion above, depending where the beam is located (on or off column) the resulting intensities in the QW may be significantly different. Therefore, depending on how the probe path was chosen the calculated profile of the integrated intensity could again vary significantly. Since the convergent angle of the incident beam (important factor for beam spreading) depends on the actual position of the specimen inside pole piece, the value used in simulations may be slightly different than the experimental value.

Another interesting observation in this and many other high resolution STEM studies at the nanometer scale is the fact that the data often fit a Gaussian function[4] [see Figs. 1(a) and 1(b) and Fig. 8]. This phenomena raises the question: Is this because the interface is not sharp or is it the result of the measurements? Three critical elements are in play here. The first and most obvious one is the width of the well. It is intuitive that with increasing width, the profile of the well (ADF intensity or EELS mapping) will look more like a rectangular function than a Gaussian. The second element is broadening of the incident beam inside the specimen. The thicker the sample the more beam broadening there will be. The third possible factor is the size of the steps in the mapping. To show the effects of all of these three factors several simulations and measurements are performed.

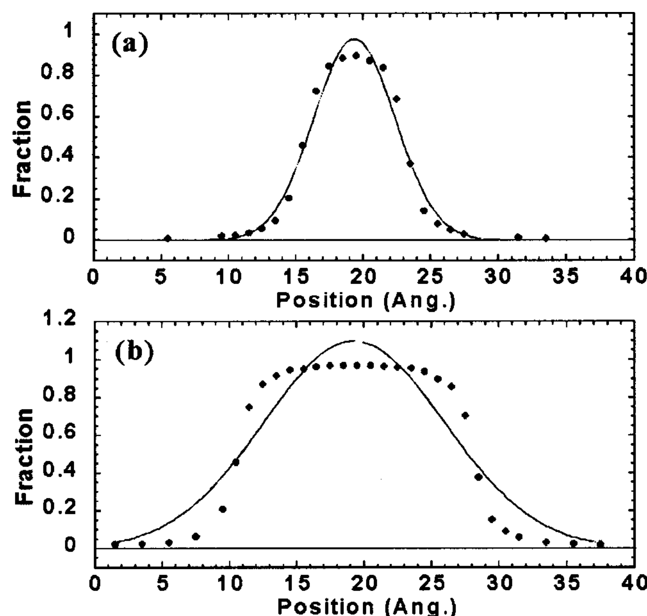

FIG. 9. Calculated fraction of the beam intensity inside the GaN QW in an AlN matrix (dots) with the best Gaussian fit (solid line): (a) original QW width of 12 Å and (b) 20 Å wide QW. The specimen was 100 Å thick in each case.

To investigate ways to minimize beam broadening, multislice simulations were undertaken for this specimen with its thickness reduced to 100 Å. The results are presented in Fig. 9(a). As can be seen, with a thinner specimen, beam broadening is reduced, and the fraction of the beam intensity inside the QW (versus incident position) visibly differs from a Gaussian fit (for comparison see Fig. 8, where a thicker sample was considered).

The effect of the width of the well can be shown by calculating the same profile of the fraction of the beam inside the QW for this specimen with a larger QW width. The results of the multislice simulations of a 20 Å QW GaN QW in an AlN matrix are presented in Fig. 9(b). The best Gaussian fit is now far off.

The last and least obvious factor is the step size between probe positions. To show this effect the results of measurements on the GaN/AlN QW from other wafer are presented. This sample contains a 10 Å GaN QW in an AlN matrix [see Figs. 10(a) and 10(b)] and the STEM specimen was about 270 Å thick. For details on this sample see Mkhoyan *et al.*[7] The composition profile due to changes of the integrated intensity of the Al $L_{2,3}$-edge across the well with ~3 Å steps fits very well to a Gaussian function [see Fig. 10(b)], while the ADF intensity taken from the same path but with finer steps, defined by the pixel size of the image, has sharper edges. To show the effect of relatively large steps, data from the ADF profile with the same steps as used with the Al $L_{2,3}$-edge are shown in Fig. 10(c). This data now fits a Gaussian function (dashed line) extremely well.

IV. POSSIBLE STRAIN EFFECTS

A report by Adelmann *et al.*[24] confirms the presence of strain in the GaN/AlN QW system, which might effect this EELS analysis. In this section, multiple-scattering (MS) and

Downloaded 16 Sep 2008 to 134.84.147.97. Redistribution subject to AIP license or copyright; see http://jap.aip.org/jap/copyright.jsp

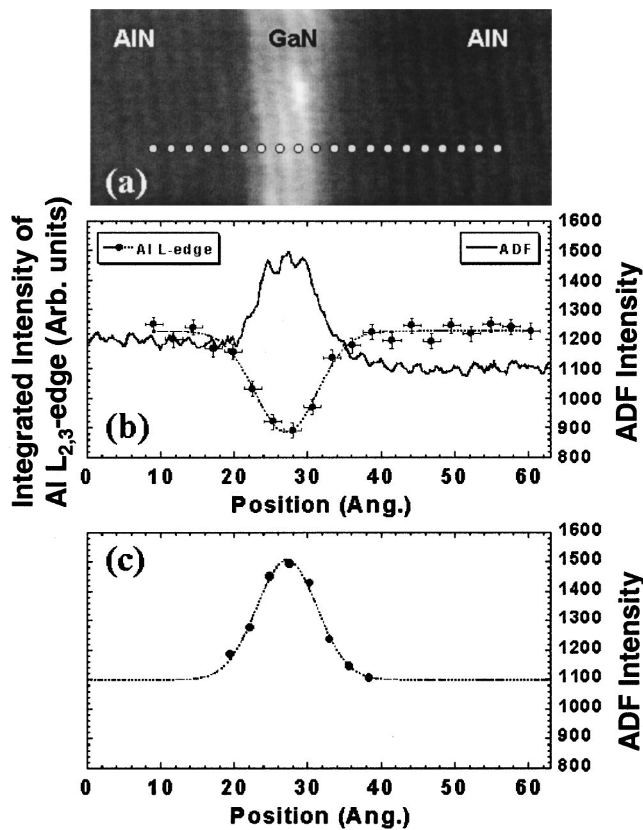

FIG. 10. (a) High magnification ADF image (with Wiener filter) of a single QW (GaN layer) with indicated probe positions (white dots), (b) integrated intensity of the Al $L_{2,3}$-edge and intensity of the ADF signal across this path. (c) Intensity of the ADF signal from (b) with the same steps used for Al $L_{2,3}$-edge. The data in (b) and (c) are fit with a Gaussian (dashed line).

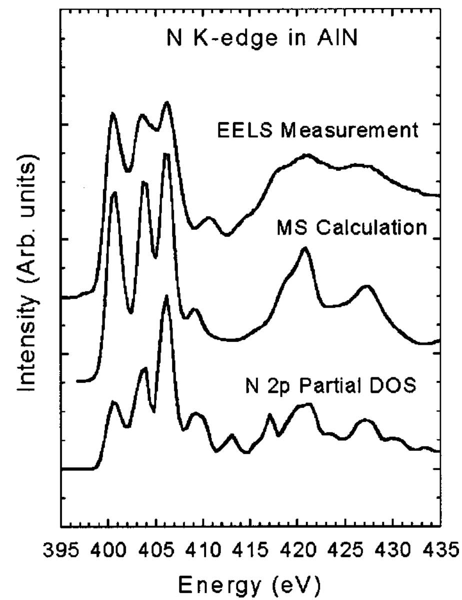

FIG. 11. Comparison of the experimental spectrum of the N *K*-edge from AlN with results of the corresponding theoretical FDMNES multiple-scattering calculations and the N $2p$ partial DOS of the conduction band calculated using VASP code.

density of states (DOS) calculations will be used to investigate strain effects on the N *K*-edge, because changes in the fine structure of this edge were used to obtain the composition profile of the QWs.

A. MS and DOS calculations

EELS and x-ray absorption spectroscopy (XAS) are similar in many ways. In each, a high energy particle (electron in EELS and photon in XAS) is incident on the atoms in the specimen. In an inelastic event, one of the electrons in a core state of an atom in the specimen is ejected into the surrounding atoms of the solid with a relatively low energy. In the multiscattering (MS) view this ejected electron undergoes multiple scattering back and forth between the surrounding atoms in the solid which affects the allowed final states of the ejected electron, and hence the near edge fine structure of the EELS and XAS absorption edge.[25] The matrix element for XAS and EELS transitions are very similar in the small scattering angle approximation (for example Egerton[12] or section 4.1 of Stöhr[26]). Despite slight differences in the cross-sections for the core-level electronic transitions excited by incident electron or x-ray beams, x-ray MS calculations can still be used to estimate the details of the fine structure in the core-level EELS.[27] The momentum transfer vector in EELS approximately corresponds to the polarization vector in XAS. Well-developed XAS simulation programs are available, and so will be used here to estimate EELS spectra.

The N *K*-edge near edge spectra in bulk AlN was calculated using the FDMNES code of Joly.[28] This program approximates the crystal potential in the *muffin-tin* approximation and uses a Green's function formalism for the multiple-scattering calculations. Acceptable convergence in the calculation of the N *K*-edge spectra was reached with the inclusion of 144 neighboring atoms. This corresponds to a spherical cluster centered on the nitrogen atom with a 7.0 Å radius. In the calculations, a 10% overlap between the spheres of the *muffin-tin* potentials was used.

The results of MS calculations for the *K*-edge in AlN are shown in Fig. 11, along with measured EELS data of the same edge. For completeness, a calculation of the N $2p$ partial density of unoccupied states (DOS) of the conduction band for AlN was also performed and the resulting curve is presented in the bottom of the Fig. 11. The N $2p$ partial DOS was calculated using density functional theory in the local density approximation as implemented by the Vienna *ab initio* Simulations Package (VASP).[29]

As can be seen from Fig. 11, while the relative positions of the peaks in the N *K*-edge of the experimental EELS data are in excellent agreement with both calculations, the correlation between the MS calculation and EELS seems better. Since the effects of the transition matrix element (albeit x-ray not EELS) as well as the DOS are reflected in MS calculations, better correlation between the EELS and the MS calculation should be expected. The excellent correlation of MS and DOS calculations with experimental EELS data can be considered as firm grounds on which to predict the expected changes of the N *K*-edge due to strain in GaN/ALN QWs.

Downloaded 16 Sep 2008 to 134.84.147.97. Redistribution subject to AIP license or copyright; see http://jap.aip.org/jap/copyright.jsp

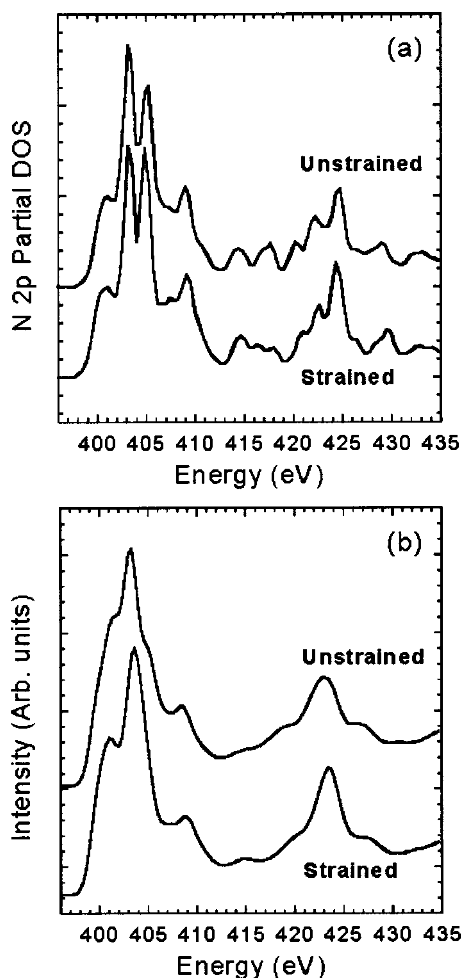

FIG. 12. (a) N $2p$ partial DOS of the conduction band in GaN with and without compressive biaxial strain with lattice constant a matched to that of the AlN (VASP results). (b) Calculated spectra of the N K-edge in GaN with and without strain using the MS method.

To investigate strain effects, consider an extreme case. The N $2p$ partial DOS of the conduction band in GaN under compressive biaxial strain with lattice constant a matched to that of the AlN was calculated using the VASP code. With lattice constant a equal to that determined for AlN, the ion positions were systematically relaxed, producing a value for the lattice constant c. The structural parameters for this biaxially strained GaN were then determined from energy minimization. The N $2p$ partial DOS was calculated for GaN with these strained structure parameters. All calculations were performed with a Monkhorst-Pack grid of $12\times12\times12$ and an energy cutoff of 40 Ry. The results of the N $2p$ partial DOS in unstrained and strained GaN are presented in Fig. 12(a). As can be seen, the effects are negligible. The results of the MS calculation on the N K-edge in GaN performed under the same strain conditions are also presented in Fig. 12(b) and indicate that possible strain induced effects on the fine structure of the N K-edge are very small.

V. CONCLUSION

In conclusion, the results of simulations together with experimental measurements suggest that beam spreading inside the specimen can significantly affect the quantitative analysis of EELS studies of QWs. Atomically sharp interfaces, as observed here, may look diffuse in STEM purely due to this beam broadening. Because beam broadening is primarily governed by penetration depth or, in other words, specimen thickness, to minimize the effects one should either use extremely thin specimens (<100 Å), or accompany measured results with appropriate simulations of beam propagation inside the specimen. In the second case the thermal vibrations of the atoms should be included in simulations.

Another critical element in the characterization of QWs is strain, and the effects that it can introduce. Multiple scattering simulations together with DOS calculations (it is important to calculate the structural parameters of the strained crystal using DOS before simulating absorption edges with the multiple scattering code) reproduce core level energy losses typically acquired in STEM and, therefore, are applicable to predictions of the strain effects on EELS.

Three major mechanisms responsible for the Gaussian profiles of QWs were discussed. While the size of the QWs is predetermined by growth, two other parameters can be considered to reduce these effects. Consideration of extremely thin samples for STEM characterization was already discussed. Mapping with very fine steps is also an option. However, e-beam induced damage of the specimen imposes strong limitations here. ADF imaging, on the other hand, typically has very high special resolution (defined by the pixel size) and produces significantly less damage to the specimen. Combination of EELS measurements at relatively large step sizes with corresponding ADF imaging is perhaps the desirable alternative.

ACKNOWLEDGMENTS

The specimen preparation facilities and the VG UHV-STEM are supported by NSF through CCMR No. DMR-9632275. The authors thank M. Thomas for technical support. This work is supported by ONR Contract No. N00014-99-10714, monitored by Dr. C. E. C. Wood.

[1] P. E. Batson and J. R. Heath, Phys. Rev. Lett. **71**, 911 (1993).
[2] D. A. Muller, T. Sorsch, S. Moccio, F. H. Baumann, K. Evans-Lutterodt, and G. Timp, Nature (London) **399**, 758 (1999).
[3] K. Suenaga, T. Tence, C. Mory, C. Colliex, H. Kato, T. Okazaki, H. Shinohara, K. Hirahara, S. Bandow, and S. Iijima, Science **290**, 2280 (2000).
[4] A. Ohtomo, D. A. Muller, J. L. Grazul, and H. Y. Hwang, Nature (London) **416**, 826 (2002).
[5] M. J. Plisch, J. L. Chang, J. Silcox, and R. A. Buhrman, Appl. Phys. Lett. **79**, 391 (2001).
[6] P. E. Batson, O. L. Krivanek, and N. Dellby, Nature (London) **418**, 617 (2002).
[7] K. A. Mkhoyan, J. Silcox, H. Wu, W. J. Schaff, and L. F. Eastman, Appl. Phys. Lett. **83**, 2668 (2003).
[8] For example, see P. E. Batson, J. Electron Microsc. **49**, 267 (2000).
[9] H. Wu, W. J. Schaff, G. Koley, M. Furis, A. N. Cartwright, K. A. Mkhoyan, J. Silcox, W. Henderson, W. A. Doolittle, and A. V. Osinsky, Mater. Res. Soc. Symp. Proc. **743**, L6.2.1 (2002).
[10] J. P. Benedict, R. Anderson, S. J. Klepeis, and M. Chaker, Mater. Res. Soc. Symp. Proc. **199**, 189 (1990).
[11] K. A. Mkhoyan, Ph.D. Thesis, Cornell University, Ithaca, NY (2004).
[12] R. Egerton, *Electron Energy Loss Spectroscopy in the Electron Microscope* (Plenum, New York, 1996).
[13] For example, see W. H. Press, S. A. Teukolsky, W. T. Vetterling, and B. P.

Downloaded 16 Sep 2008 to 134.84.147.97. Redistribution subject to AIP license or copyright; see http://jap.aip.org/jap/copyright.jsp

Flannery, *Numerical Recipes in C* (Cambridge University, Cambridge, England, 1997).
[14] K. Lawniczak-Jablonska, T. Suski, Z. Liliental-Weber, E. M. Gullikson, J. H. Underwood, R. C. C. Perera, and T. J. Drummond, Appl. Phys. Lett. **70**, 2711 (1997).
[15] V. Serin, C. Colliex, R. Brydson, S. Matar, and F. Boucher, Phys. Rev. B **58**, 5106 (1998).
[16] J. M. Cowley and A. F. Moodie, Acta Crystallogr. **10**, 609 (1957).
[17] E. J. Kirkland, R. F. Loane, and J. Silcox, Ultramicroscopy **23**, 77 (1987).
[18] J. Silcox, P. Xu, and R. F. Loane, Ultramicroscopy **47**, 173 (1992).
[19] R. F. Loane, P. Xu, and J. Silcox, Acta Crystallogr. **A47**, 267 (1991).
[20] D. A. Muller, B. Edward, E. J. Kirkland, and J. Silcox, Ultramicroscopy **86**, 371 (2001).
[21] E. J. Kirkland, *Advanced Computing in Electron Microscopy* (Plenum, New York, 1998).
[22] R. F. Loane, E. J. Kirkland, and J. Silcox, Acta Crystallogr., Sect. A: Found. Crystallogr. **A44**, 912 (1988).
[23] S. Hillyard, R. F. Loane, and J. Silcox, Ultramicroscopy **49**, 14 (1993).
[24] C. Adelmann, E. Sarigiannidou, D. Jalabert, Y. Hori, J.-L. Rouviere, B. Daudin, S. Fanget, C. Bru-Chevallier, T. Shibata, and M. Tanaka, Appl. Phys. Lett. **82**, 4154 (2003).
[25] J. J. Rehr and R. C. Albers, Rev. Mod. Phys. **72**, 621 (2000).
[26] J. Stöhr, *NEXAFS Spectroscopy* (Springer, Berlin, 1996)
[27] M. Isaacson and M. Utlaut, Optik (Jena) **50**, 213 (1978).
[28] Y. Joly, Phys. Rev. B **63**, 125 120 (2001).
[29] G. Kresse and J. Hafner, Phys. Rev. B **47**, RC558 (1993); G. Kresse and J. Furthmüller, Comput. Mater. Sci. **6**, 15 (1996); G. Kresse and J. Furthmüller, Phys. Rev. B **54**, 11 169 (1996).

Downloaded 16 Sep 2008 to 134.84.147.97. Redistribution subject to AIP license or copyright; see http://jap.aip.org/jap/copyright.jsp